Hydrogen solubility of stishovite provides insights into water transportation to the deep Earth

Mengdan Chen, Changxin Yin, Danling Chen, Long Tian, Liang Liu, and Lei Kang

Department of Geology, Northwest University/State Key Laboratory of Continental Dynamics, Xi'an, 710069, China

Correspondence: Lei Kang (kanglei@nwu.edu.cn)

Abstract. Water dissolved in nominally anhydrous minerals (NAMs) can be transported to deep regions of the Earth through subducting slabs, thereby significantly influencing the physicochemical properties of deep-Earth materials and impacting dynamic processes in the deep Earth. Stishovite, a prominent mineral present in subducting slabs, remains stable at mantle pressures of 9–50 GPa and can incorporate various amounts of water (H^+, OH^-, and H_2O) in its crystal structure. Consequently, stishovite can play a crucial role in transporting water into the deep Earth through subducting slabs. This paper provides a comprehensive review of the research process concerning water (hydrogen) solubility in stishovite. The key factors that govern water solubility in stishovite are summarized as temperature, pressure, water fugacity, and aluminum content. Combined with published results on the dependence of water solubility on the aforementioned parameters, this paper proposes a new equation to describe the solubility of water in Al-bearing stishovite. Calculation results based on this equation suggest that stishovite may effectively accommodate water released from processes such as hydrous mineral breakdown, which could ultimately contribute to the presence of a water-rich transition zone.

1 Introduction

Water plays a crucial role not only in the origin and evolution of life but also in various Earth processes, including slab subduction, crust–mantle reaction, and recycling. During slab subduction, water is transported from the Earth's surface to its interior through subduction zones, and a significant amount of water returns to the surface mainly through magmatism, thus forming a large-scale water cycle (Fig. 1).
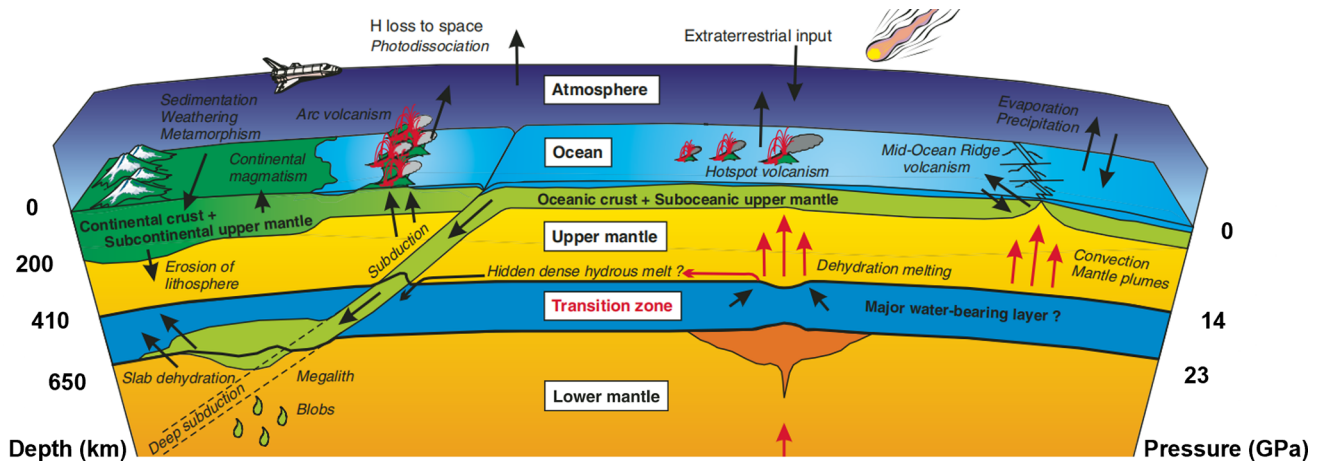
In subducting slabs, hydrogen exists in melts, fluids, fluid inclusions, hydrous minerals (e.g., amphibole and mica), and nominally anhydrous minerals (NAMs) (Bell et al., 1995; Rossman, 1996; Xia et al., 1998; Johnson, 2006; Libowitzky, 2006; Litasov and Ohtani, 2007; Ni et al., 2017) in forms of both molecular water (H_2O) and structurally bound water (H_3O^+, H^+, and OH^-). Most hydrous minerals in subducting slabs decompose and release water before reaching a depth of 300 km (Poli and Schmidt, 2002). Part of this water returns to the surface through magmatism, while the remainder is incorporated into NAMs in ultrahigh-pressure metamorphic rocks (Magni et al., 2014; Walter, 2021) and subsequently transported to deep mantle by subducting slabs (Ishii et al., 2022).

Numerous studies indicate that major constituent minerals in deep mantle, such as olivine, pyroxene, and garnet, as well as their high-pressure polymorphs, are NAMs (Litasov and Ohtani, 2007; Liu et al., 2016). Although the phase of SiO_2 does not typically appear in the mantle (Kaminsky, 2012), it is a significant constituent mineral in silica-rich slabs and can stably exist at upper to lower mantle depths through high-pressure polymorphic phase transitions (Fig. 2). Both experimental and computational studies have demonstrated that stishovite can incorporate a certain amount of water. Given its prevalence as a major mineral in subducting slabs at mantle depths (> 300 km), stishovite likely plays a significant role in water transportation to the deep Earth (Spektor et al., 2011; Lin et al., 2022; Ishii et al., 2022). In this paper, we provide a systematic review of previous understandings and the research process regarding water solubility, water incorporation mechanisms, and factors influencing water solubility in stishovite. Considering stishovite in subducting slabs always contains amounts of Al in its crystal structure (Ono,

Figure 1. Water transport, distribution, and cycling in the Earth (Litasov and Ohtani, 2007).
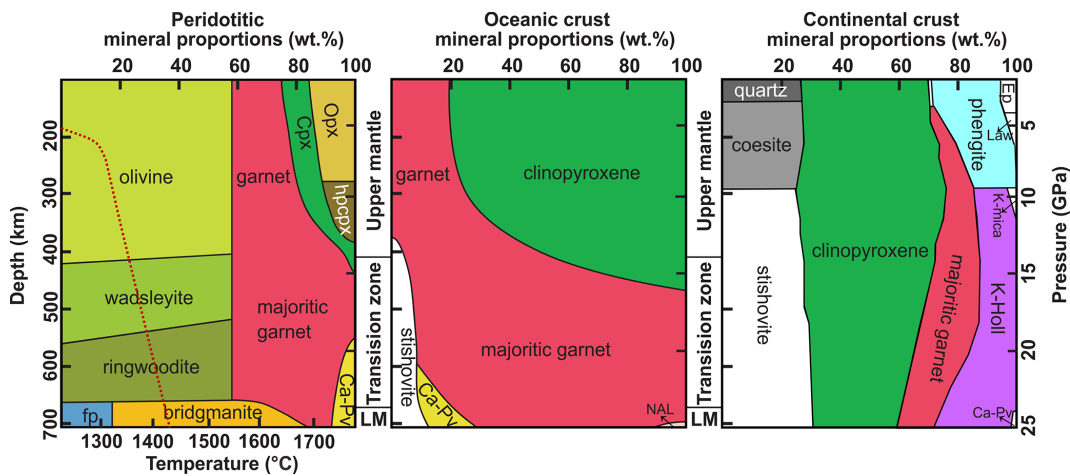

Figure 2. Mineral assemblages in peridotite, subducted oceanic crust, and subducted continental crust. The red line indicates the mantle geotherm (Kaminsky, 2012). Modified after Smith et al. (2018) and Wu et al. (2009). Fp – ferropericlase; Opx – orthopyroxene; Cpx – clinopyroxene; Ca-pv – Ca-perovskite; NAL – Na–Al phase; Ep – epidote; Law – lawsonite; K-Holl – K-hollandite.

1999; Lakshtanov et al., 2007a), this paper establishes an empirical model for water solubility in Al-stishovite based on published results and discusses the significance of stishovite in transporting water from subducting slabs to the deep mantle and its implications for deep-Earth dynamics. Finally, we highlight key unresolved scientific questions in the research on water solubility in stishovite.

2   Crystal structure and stability of stishovite

The phase of SiO_2 undergoes multiple high-pressure polymorphic transitions as pressure increases (Petersen et al., 2021) (Fig. 3). Under a subduction slab geothermal gradient, coesite is the dominant phase of SiO_2 at pressures ranging from 2.7 to 9 GPa. At approximately 10 GPa, coesite transforms into denser stishovite (Ono et al., 2017). The transition pressure from coesite to stishovite is de-

pendent on temperature, as described by the equation P (GPa) $= 4.7 + 0.0032 \times T$ (K) (Ono et al., 2017). This phase transition is believed to contribute to the seismic discontinuity observed at around 300 km depth (Ono et al., 2017). As pressure increases further to ~ 24 GPa, stishovite undergoes a transformation into the $CaCl_2$-type SiO_2 structure (commonly referred to as post-stishovite) due to the incorporation of Al and H in stishovite (Ishii et al., 2022). However, the transition pressure is still debated. Fischer et al. (2018) pointed out that the phase transition between stishovite and $CaCl_2$-type silica should occur at pressures of 68–78 GPa in the Earth, depending on the temperature in subducting slabs.

Previous studies show that stishovite constitutes 10 vol. % and 20 vol. % of subducting mid-ocean ridge basalt (MORB) in the upper and lower mantle, respectively (Irifune et al., 1986; Ono et al., 2001). In subducted continental crust at up-
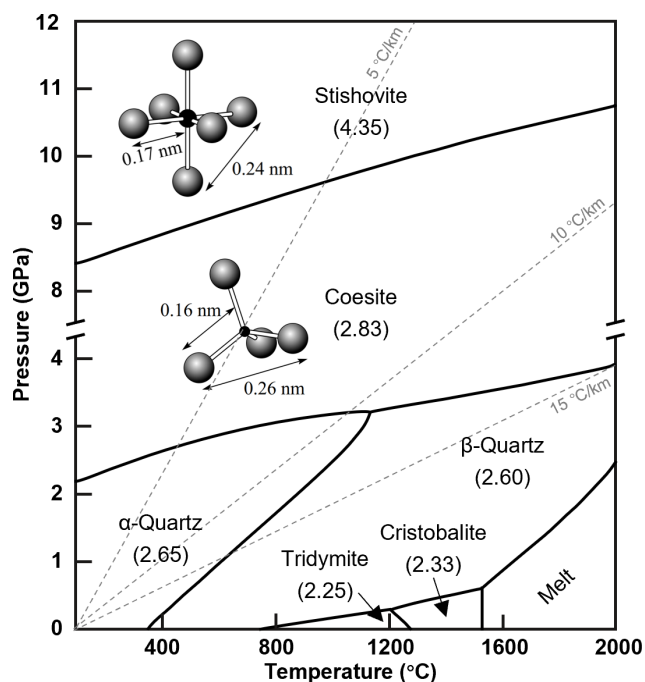
Figure 3. SiO$_2$ phase diagram as recommended in the reference literature (density values are indicated in parentheses) (Gutzow et al., 2014). The dashed gray line represents the subduction slab geothermal gradient (Zheng et al., 2016). The diagram also illustrates the SiO$_4$ tetrahedron and SiO$_6$ octahedron, along with their corresponding distances.

per mantle depths (< 660 km), stishovite can reach approximately 20 vol. %–25 vol. % (Irifune et al., 1994; Poli and Schmidt, 2002; Ishii et al., 2012). However, due to the fact that the exhumation of subducted slabs from ~ 300 km depth (termed the "depth of no return" in the literature, e.g., Irifune et al., 1994; Liu et al., 2007; Wu et al., 2009) to the surface is extremely difficult, and stishovite is unstable and easily transforms to lower-pressure SiO$_2$ polymorphs, naturally formed stishovite that can be observed is extremely rare. Previously, Yang et al. (2007) identified polycrystalline coesite as a potential pseudomorphic replacement of stishovite in Tibetan chromitites. The exsolution microstructure (Liu et al., 2007) and pseudomorphs after stishovite (Liu et al., 2018) were found in the South Altyn ultrahigh-pressure metamorphic belt in western China. Recently, Thomas et al. (2022) identified coesite and stishovite inclusions in the Waldheim granulite, and Gu et al. (2022) showed that coesite (former stishovite) was present within a natural super-deep diamond formed at the boundary between the transition zone and the lower mantle. In addition, other naturally occurring stishovite is found sporadically in meteorite impact craters (e.g., Chao et al., 1962) or meteorites (e.g., Holtstam et al., 2003). Therefore, our current understanding of stishovite mainly relies on high-temperature and high-pressure experiments and theoret-

ical calculations (e.g., Litasov et al., 2007; Lin et al., 2022; Ishii et al., 2022).

Stishovite was first synthesized by Stishov and Popova (1961) at 20 GPa (equivalent to approximately 600 km depth in the Earth's interior) and 1100 °C from α-quartz. It possesses a rutile-type structure with tetragonal symmetry ($P4_2/mnm$). The Si atoms are coordinated by six O atoms in octahedral arrangements (Pawley et al., 1993; Spektor et al., 2011; Lin et al., 2022). These SiO$_6$ octahedra align and form linear chains along the c axis. This arrangement results in a highly dense packing of O atoms, with slightly elongated Si–O bonds compared to SiO$_4$ tetrahedra. Previous studies have demonstrated that the density of stishovite is 46 % higher than coesite and 60 % higher than α-quartz (Keskar et al., 1991). Therefore, the formation of stishovite during slab subduction at depths exceeding 300 km can dramatically increase the density of subducting slabs (Lin et al., 2022; Ishii et al., 2022) and enhance their negative buoyancy for further subduction into the mantle transition zone (MTZ) (410–660 km) or even deeper regions.

3 Water solubility and incorporation mechanisms in stishovite

3.1 Water solubility

Research on water solubility in stishovite has primarily been conducted through high-pressure experiments (Chung and Kagi, 2002; Bromiley et al., 2006; Litasov et al., 2007; Spektor et al., 2011; Nisr et al., 2017; Lin et al., 2022; Ishii et al., 2022). Fourier transform infrared spectroscopy (FTIR) is the primary technique used to determine water content in experimental products, although results from different studies often show significant discrepancies, as detailed in Yan et al. (2021). In this paper, we compile the experimental conditions (temperature, pressure, and initial water content) and results (water and Al$_2$O$_3$ content in stishovite products) from previous studies (Table 1).

As shown in Table 1, water solubility in stishovite is significantly influenced by temperature, pressure, and Al content, with large variations from a few parts per million to a few weight percent. However, even under specific pressure conditions, water content obtained by different studies can differ by more than 1 order of magnitude. For example, at 20–25 GPa, some studies obtained 25–2700 wt ppm water (Litasov et al., 2007; Y. Zhang et al., 2022), while others reported 0.5–3 wt % water (Spektor et al., 2011, 2016). These discrepancies may partially be attributed to different water content measurement methods. In Table 1, it can be seen that most FTIR studies yielded water content at the weight in parts per million level, while other methods yielded water content at the weight percent level. For example, Nisr et al. (2017, 2020) suggested a calibration based on unit cell

Table 1. Water content in stishovite from previous studies.

Temperature (°C)	Pressure (GPa)	Initial water content (wt %)	Synthesis method	Al_2O_3 (wt %)	Water content (wt ppm)	Measurement method	References
1200	10	saturated	LVP	0–1.51	7–82	FTIR[a]	Pawley et al. (1993)
1200–1500	15–21	saturated	LVP	0	2.5–72	FTIR[b]	Bolfan-Casanova et al. (2000)
1200–1400	10–15	saturated	LVP	0.612–1.341	210–759	FTIR[b]	Chung and Kagi (2002)
1740–3700	30–62.9	0.2	DAC	unspecified	76–487	FTIR[a]	Panero et al. (2003)
1227	25	saturated	unspecified	unspecified	3000	DFT	Panero and Stixrude (2004)
1500	15	saturated	LVP	0–2.95	3–456	FTIR[a]	Bromiley et al. (2006)
1800	20–25	saturated	LVP	0–7.62	25–3010	FTIR[b]	Litasov et al. (2007)
800–1240	8–12.3	1–4	LVP	trace	53–187	FTIR[c]	Thomas et al. (2009)
450–550	10	saturated	LVP	0	0.9 wt %–1.75 wt %	TGA and SIMS	Spektor et al. (2011)
627–1654	12	0–1.73	LVP	0–2.24	108–1354	FTIR[b]	Yoshino et al. (2014)
350–550	10	unspecified	LVP	0	0.5 wt %–3 wt %	TGA	Spektor et al. (2016)
450	9	unspecified	LVP	0	3.2 wt %	LP	Nisr et al. (2017)
950	8.4–9.1	1.5–6	LVP	unspecified	246–376	FTIR[c]	Frigo et al. (2019)
967–1562	32.5–52	unspecified	DAC	0	4.6 wt %–9.9 wt %	From Nisr et al. (2017)	Lin et al. (2020)
1700	20	saturated	LVP	3.43–5.37	2500–2700	FTIR[b]	Y. Zhang et al. (2022)
1700	28	saturated	LVP	4.36	2700	FTIR[b]	Ishii et al. (2022)
973–1592	53–72.5	0.5–15.2	DAC	0	0.62 wt %–3.61 wt %	DFT	Lin et al. (2022)
450	9	8	LVP	0	1.57 wt %–2.25 wt %	LOI average	Kueter et al. (2023)
1627	23	saturated	LVP	0	0.43 wt %–0.62 wt %	nano-SIMS/NMR	Li et al. (2023)

Note: DAC, diamond anvil cell; LVP, large-volume press; TGA, thermogravimetric analysis; SIMS, secondary ion mass spectrometry; LP, water content determined from lattice parameters; DFT, density functional theory calculation; LOI, loss on ignition; nano-SIMS/NMR, nanoscale secondary ion mass spectroscopy and solid-state nuclear magnetic resonance. [a] Calculation methods of water content based on FTIR from Pawley et al. (1993). [b] Calculation methods of water content based on FTIR from Paterson (1982). [c] Calculation methods of water content based on FTIR from Libowitzky and Rossman (1997).

volume dependency on water in stishovite from density functional theory (DFT) calculations. Lin et al. (2020) applied Nisr et al.'s (2017) formulation to calculate H_2O content in their high-pressure samples, resulting in exceptionally high H_2O concentrations exceeding 10 wt % in many instances. However, Lin et al. (2022) noted that estimating H_2O content using unit cell volumes from samples synthesized in either the large-volume press (LVP) or the diamond anvil cell (DAC) is highly uncertain.

Additionally, the discrepancies may relate to variations in experimental conditions of temperature and Al content in stishovite, as detailed in Sect. 4.

3.2 Hydrogen incorporation mechanisms

Previous studies indicate two primary mechanisms for water incorporation in stishovite: (1) "hydrogarnet" substitution by $4H^+ \rightarrow Si^{4+}$ and (2) coupled substitution of H^+ and Al^{3+} for Si^{4+} ($Al^{3+} + H^+ \rightarrow Si^{4+}$). Hydrogarnet substitution is a common mechanism in pure stishovite. Studies by Litasov et al. (2007) have shown that stishovite can dissolve up to 5 wt % Al_2O_3, which can further increase to 9 wt % with the presence of water (Ono, 1999). Numerous high-pressure experiments demonstrate that Al can directly couple with H by substituting Si to increase water solubility in Al-bearing stishovite, with the coupled substitution mechanism of $Al^{3+} + H^+ \rightarrow Si^{4+}$ (Pawley et al., 1993; Chung and Kagi, 2002; Bromiley et al., 2006; Lakshtanov et al., 2007a). In addition to Al^{3+}, stishovite contains minor quantities of other

trivalent cations such as B^{3+}, Fe^{3+}, V^{3+}, and Cr^{3+}, which can also facilitate H incorporation into the stishovite structure by similar mechanisms to Al^{3+} (Irifune and Ringwood, 1993; Pawley et al., 1993). However, Litasov et al. (2007) found that H^+ (OH) can only co-replace Si^{4+} with up to 40 % Al^{3+}, which makes the Al / H ratio in stishovite far greater than 1 / 1; that is, Al in stishovite is much higher than H. Bromiley et al. (2006) also reported excess Al in stishovite, not charge balanced by hydrogen. Thus, the incorporation of aluminum cannot be explained solely by the charge-coupled substitution with protons in stishovite, and other substitution mechanisms have also been proposed. For instance, most Al will occupy the oxygen vacancy (O_V) and balance the charge by $2Al^{3+} + O_V^{2+} \rightarrow 2Si^{4+}$ (Pawley et al., 1993; Chung and Kagi, 2002; Litasov et al., 2007; Y. Zhang et al., 2022).

Recently, molecular water (H_2O) has been identified in stishovite (Lin et al., 2020, 2022; Kueter et al., 2023). The incorporation mechanism is summarized as interstitial H_2O substitution (Lin et al., 2022). Li et al. (2023) presented a new mechanism (one-dimensional (1D) water channels) for molecular water incorporation into stishovite using high-dimensional neural network (HDNN) potential. Both mechanisms for incorporation of molecular water could explain the weight percent level water observed in Al-free stishovite. Notably, the initial material in these studies is pure SiO_2, which means H is impossible coupled with Al to substitute Si. Therefore, even though multiple substitution mechanisms exist for H incorporation in stishovite, the dominant mech-

anisms in the natural environment remain highly uncertain (Lin et al., 2022). Due to the fact that stishovite in subducting slabs contains Al, as mentioned above (e.g., Litasov et al., 2007), we emphasize that $Al^{3+} + H^+ \rightarrow Si^{4+}$ is still very important (e.g., Pawley et al., 1993; Chung and Kagi, 2002; Lakshtanov et al., 2007a; Y. Zhang et al., 2022; Ishii et al., 2022).

# 4 Factors dominating water solubility in stishovite

4.1 Temperature and pressure

Numerous experiments have constrained the water solubility in Al-bearing stishovite as a function of temperature and pressure. Panero et al. (2003) showed that at 30–38 GPa, water content in stishovite significantly increases with increasing temperature from ∼ 100 wt ppm at 1500 K to 400 wt ppm at 3500 K. Litasov et al. (2007) measured the hydrogen content of stishovite samples synthesized at 20–25 GPa and 1200–1800 °C from several starting materials containing up to 10 wt % Al_2O_3 and found that H_2O content is positively correlated with temperature between 1000 and 1200 °C but decreases with increasing temperature at 1200–1800 °C. This can be simply explained by the fact that hydrogen, as an incompatible element, preferably dissolves into the melt (Smyth, 2006; Litasov et al., 2007). Therefore, the occurrence of melt at high temperature can significantly reduce H_2O content in stishovite. Panero et al. (2003) showed that at 10–60 GPa, water solubility in stishovite increases with increasing pressure. Panero and Stixrude (2004) suggested that the water solubility in stishovite is ∼ 0.3 wt % H_2O at 25 GPa and 1500 K and increases to 1.15 wt % H_2O at 60 GPa, indicating increasing solubility with pressure. By comparing previous studies, it is evident that water solubility in Al-bearing stishovite shows an overall weak positive correlation with temperature but a significant decrease when the melt is present at > 1600 °C, whereas the pressure dependence is more complex, with a positive correlation below 20 GPa but a negative correlation above 20 GPa, suggesting an optimal water solubility in stishovite at ∼ 20 GPa (Fig. 4). In addition, Lakshtanov et al. (2007b) suggested that stishovite undergoes a transition to the $CaCl_2$-structured phase (post-stishovite) at ∼ 30 GPa. Weight percent levels of water (0.85 wt % to 1.1 wt %) in $CaCl_2$-structured, Al-rich post-stishovite at 24 to 28 GPa and 1000 to 2000 °C were reported by Ishii et al. (2022). This implies stishovite can retain its water content through phase transition with increasing pressure. However, Fischer et al. (2018) suggested the transition to post-stishovite occurs at pressures of 68–78 GPa in the Earth. Therefore, it remains unclear if the post-stishovite can accommodate water at ∼ 20 GPa where the Al-bearing stishovite has a peak water solubility.

4.2 Al content

Given that natural systems always contain some Al, its effect on water solubility in stishovite has been a focus of research. Pawley et al. (1993) found that for stishovite with > 1 wt % Al_2O_3, the H_2O content (82 wt ppm) is 10 times higher than Al-free stishovite (7 wt ppm). Chung and Kagi (2002) showed that at 15 GPa and 1400 °C, with increasing trivalent cations (mostly Al) from 0.612 wt % to 1.341 wt %, H_2O content in stishovite increases from within the range of 128 to 536 wt ppm. Litasov et al. (2007) obtained the maximum 3010 wt ppm H_2O in Al-bearing stishovite (4.4 wt % Al_2O_3) versus 16–30 wt ppm H_2O in Al-free stishovite at 20 GPa and 1400 °C. Recent work by Ishii et al. (2022) also demonstrated the positive correlation between water solubility and Al_2O_3 content in stishovite. Therefore, increasing Al significantly enhances water solubility in stishovite. Previous data demonstrate a positive correlation between Al and water content in stishovite (Fig. 5).

In contrast, Lin et al. (2022) showed decreasing water solubility in pure stishovite with increasing temperature and pressure, markedly different from Al-bearing systems. Also, Lin et al.'s (2022) experimental data indicate an H_2O storage capacity in Al-free stishovite of ∼ 3.5 wt % at ∼ 50 GPa and 1800 K. Kueter et al. (2023) reported that Al-free stishovite contains on average 1.69 wt % water at 9 GPa and 450 °C. However, previous LVP studies synthesized Al-free (or Al-poor at the weight in parts per million level) stishovite under water-saturated conditions and found it to be nearly anhydrous and commonly containing less than 100 wt ppm H_2O, which is significantly different from the weight percent of H_2O in recent studies (e.g., Spektor et al., 2011, 2016; Lin et al., 2022; Kueter et al., 2023). It is challenging to understand how different studies can produce such widely disparate results, with differences of several orders of magnitude for the H_2O capacity of stishovite (Lin et al., 2022). The reason for the difference is unclear, and there are various possible explanations. One possible cause is water loss from the capsule (e.g., Litasov et al., 2007). Moreover, the large discrepancy of water solubility between Al-stishovite (weight in parts per million level) and Al-free stishovite (weight percent level from recent studies) has partly been explained by a hydrogarnet substitution mechanism ($Si^{4+} \leftrightarrow 4H^+$) and/or the incorporation of interstitial molecular water (Kueter et al., 2023). However, the discrepancy caused by different measurement methods should be taken into consideration as well.

It should be noted that the behavior of Al itself also depends on pressure and temperature. Al can remarkably increase the hydrogen solubility of stishovite (Fig. 5), and hydrogen can also increase Al solubility of stishovite in return. However, previous studies mainly focus on the water solubility of Al-free or Al-saturated stishovite. Studies on the P–T dependence of Al solubility in stishovite are very limited (e.g., Liu et al., 2006; Litasov et al., 2007). Liu et al. (2006) investigated Al solubility in dry stishovite in an-
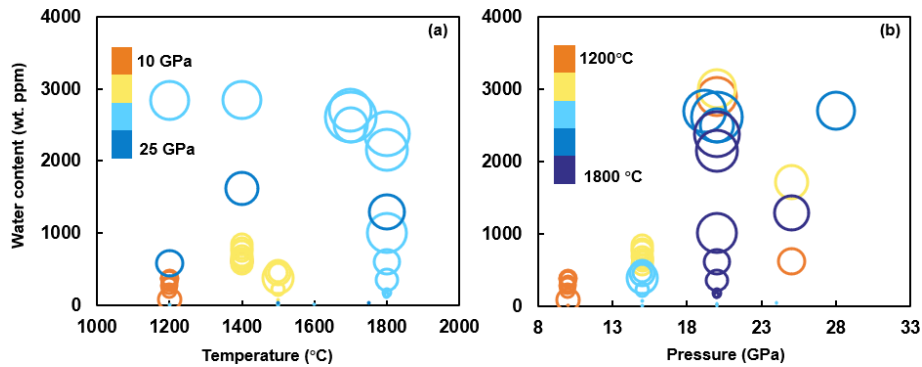
Figure 4. Previous studies on water solubility in Al-bearing stishovite. The dimension of circles represents the Al content. While panel **(a)** depicts water content versus temperature, panel **(b)** depicts water content versus pressure. Only FTIR data are presented (data from Pawley et al., 1993; Chung and Kagi, 2002; Bromiley et al., 2006; Litasov et al., 2007; Ishii et al., 2022; Y. Zhang et al., 2022). The correlation between water solubility and Al content is shown in Fig. 5.
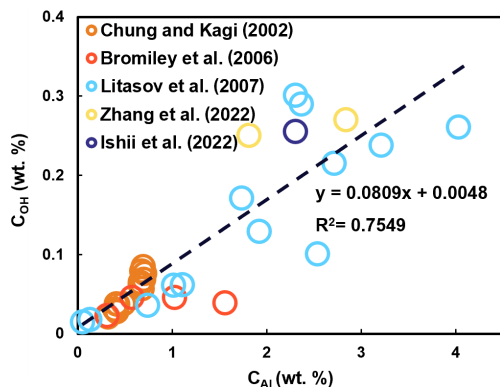
Figure 5. The correlation between H_2O and Al_2O_3 in stishovite. Data are from Chung and Kagi (2002), Bromiley et al. (2006), Litasov et al. (2007), Ishii et al. (2022), and Y. Zhang et al. (2022). In Al-free stishovite, water content ranges from 0.0003 wt %–0.0108 wt % (3–108 wt ppm). In Al-bearing stishovite, water content increases to 0.0082 wt %–0.301 wt % (82–3010 wt ppm) with increasing Al.

hydrous experiments at 15–25 GPa and 1350–2150 °C. Liu et al. (2006) found that Al_2O_3 solubility in dry stishovite is slightly but consistently reduced by pressure increase; however, its response to temperature increase is more complicated. It increases at low temperatures, maximizes at around 2000 °C, and perhaps decreases at higher temperatures. Therefore, quantitatively constraining water solubility in natural stishovite requires considering Al solubility under different $P–T$ conditions. In summary, the role of Al and other impurities in the water content and stability of hydrous stishovite remains poorly understood (Kueter et al., 2023).

4.3 Other factors

Apart from aluminum (Al), other impurity ions likely play a role in affecting water solubility in stishovite. Several studies

(Ono et al., 2002; Chung and Kagi, 2002; Panero et al., 2003; Panero and Stixrude, 2004) have suggested that stishovite formed from subducted MORB might incorporate a variety of trivalent cations, such as Al^{3+}, Cr^{3+}, Fe^{3+}, V^{3+}, and Ti^{3+}. These cations could potentially increase water content through coupled substitution. However, the work of Litasov et al. (2007) reported a small discrepancy in the H_2O content between Fe-bearing stishovite (likely containing Fe^{3+}) and Al-free and Fe-free stishovite. Consequently, the implications of Fe^{3+}, Ti^{3+}, and other elements for water solubility in stishovite need further investigation.

In addition, oxygen fugacity (fO_2) stands as a crucial thermodynamic parameter that describes the oxidation state in the deep Earth. It has a strong impact on the water solubility of those NAMs containing valency elements (e.g., Fe and Ti). For instance, the water solubility in olivine and garnet displays positive and negative correlations, respectively, with fO_2 (Yang, 2016; K. Zhang et al., 2022). Since a small amount of Fe and Ti is determined in a pseudomorph of former stishovite from a continental subduction slab (Liu et al., 2018), fO_2 could theoretically affect the water solubility of stishovite. However, the fO_2 dependence on water solubility of stishovite remains unknown and requires further investigation to provide clear insights.

5   Water solubility in stishovite as a function of pressure, temperature, water fugacity, and Al content

Numerous studies have revealed that the water content in NAMs basically follows a thermodynamic relationship with temperature, pressure, and water fugacity as shown in Eq. (1) (e.g., Kohlstedt et al., 1996; Zhao et al., 2004; Karato, 2010):

$$C_{OH} = A \cdot f_{H_2O}^n \cdot \exp\left(-\frac{\Delta E + \Delta V \cdot P}{R \cdot T}\right), \tag{1}$$

where C_{OH} is the water content, A is a constant, $f_{H_2O}^n$ is the water fugacity, the value of n depends on the hydrogen incorporation mechanism, and ΔE and ΔV denote the energy and volume changes associated with hydrogen dissolution.

Lin et al. (2022) suggested that water solubility in Al-free stishovite is related to pressure and temperature. Considering that stishovite in a subducted slab contains up to 5 % Al (Litasov et al., 2007) and that aluminum (Al) has a remarkable influence on the hydrogen solubility of stishovite ($Al^{3+} + H^+ \rightarrow Si^{4+}$), we therefore propose a new model for water solubility in Al-bearing stishovite as Eq. (2):

$$C_{OH}^{St} = A \cdot f_{H_2O}^n \cdot \exp\left(-\frac{\Delta E + \Delta V \cdot P}{R \cdot T}\right) \cdot \exp\left(\frac{B \cdot X_{Al}}{R \cdot T}\right). \quad (2)$$

In Eq. (2), C_{OH}^{St} is water solubility in Al-bearing stishovite, B is a constant, and X_{Al} is the molar fraction of Al in stishovite. The dominant hydrogen incorporation mechanism corresponds to $Al^{3+} + H^+ \rightarrow Si^{4+}$ (Pawley et al., 1993), yielding $C_{OH}^{St} \propto f_{H_2O}^{0.5}$; thus $n = 0.5$ (Kohlstedt et al., 1996; Karato, 2010).

To eliminate large disparities arising from diverse analytical methods as discussed above, we excluded the published water solubility in Al-bearing stishovite obtained by methods such as thermogravimetric analysis (TGA) and secondary ion mass spectrometry (SIMS) and only collected H_2O solubility from FTIR measurements (Chung and Kagi, 2002; Litasov et al., 2007; Ishii et al., 2022; Y. Zhang et al., 2022, as shown in Table 1). We used a non-linear least square fitting method to fit Eq. (2) and obtained parameters as follows: $n = 0.5$, $A = 24 \pm 13$ ppm GPa$^{-0.5}$, $\Delta E = -3.06 \pm 0.88$ kJ mol^{-1}, $\Delta V = 4.29 \pm 0.27$ cm^3 mol^{-1}, and $B = 7.69 \pm 1.12$ kJ mol^{-1}. The uncertainty is 1 standard deviation. As shown in Fig. 6, a very good correlation can be found between the experimental data and the calculated results from Eq. (2) (Fig. A1). Due to the fact that the data we used to fit Eq. (2) are from experiments carried out under wide conditions of 10–28 GPa and 1200–1800 °C (close to the condition of the MTZ), Eq. (2) can now reasonably estimate the water solubility in Al-bearing stishovite across temperature, pressure, and f_{H_2O} conditions of the MTZ.

We performed calculations to determine the water solubility in stishovite containing 3 mol % aluminum at temperatures ranging from 800 to 1600 °C and pressures from 10 to 40 GPa (Fig. 6). The results indicate that up to 30 GPa, water content experiences a marginal decline as temperature rises, while beyond 30 GPa, a positive correlation emerges between water content and temperature. This could be attributed to a lowered solidus under reduced pressures, leading to diminished water solubility as high-temperature, water-rich melts form. Conversely, at pressures surpassing 30 GPa, the heightened solidus counteracts the melt effect. Moreover, the solubility of water experiences a marked increase at pressures below 22 to 32 GPa, followed by a decrease at pressures beyond this range, signifying an optimal solubility window.

This aligns well with the overarching experimental data trend (Fig. 6b).

6 Implications for water transport to the deep Earth

Subduction zones serve as the exclusive pathway for surface water to infiltrate the Earth's deep interior. The transport and quantities of water within subducting slabs have profound impacts on surface environments and deep-Earth properties and dynamics (Shillington, 2018). Existing experimental and geophysical data suggest the mantle transition zone distributes potentially water-rich regions with > 1 wt % H_2O (Pearson et al., 2014). However, the origins of this water remain a subject of debate. One perspective posits that the deep mantle has retained intrinsic wetness since the Earth's formation. Alternatively, NAMs in subducting slabs may carry a significant amount of water to the deep mantle (Peslier et al., 2017). However, it is essential to note that most hydrous minerals within subducting slabs will break down at various depths, typically having stability limits below 9 GPa, which limits the transport of water to greater mantle depths (> 300 km) (Zheng et al., 2016). For instance, minerals like antigorite, phlogopite and lawsonite, which can survive to maximum depths in cold slabs, tend to dehydrate at around 300 km (Poli and Schmidt, 2002; Walter, 2021). Therefore, a fundamental question arises: can the released water from these hydrous minerals be further carried to even greater depths by NAMs?

Existing research demonstrates that water storage capacities within upper-mantle NAMs generally increase with depth (Yang and Li, 2016). Nevertheless, it is imperative to investigate how phase transitions and breakdown reactions of NAMs influence the transport of water in subducting slabs at greater depths. For instance, Gavrilenko (2008) showed that water solubility in clinopyroxene (Cpx) decreases along a mantle geotherm (Litasov and Ohtani, 2007) from 517 wt ppm at 10 GPa to 176 wt ppm at 16 GPa. Given the concurrent decomposition of Cpx from approximately 65 vol. % at 9 GPa to 0 vol. % at 16 GPa, an estimated 310 wt ppm of water would be released from Cpx within the subducted oceanic slab.

We further conducted calculations to assess the evolution of water storage capacities in major minerals within subducted MORB and continental sediments along a cold subduction slab geotherm suggested by Litasov and Ohtani (2007). The results indicate that garnet and stishovite serve as primary carriers of water, with higher water storage capacities observed in subducted oceanic crust compared to sediments (Fig. 7). In subducted MORB and continental sediments down to mantle depths, stishovite comprises 10 vol. %–20 vol. % (Irifune et al., 1986; Ono et al., 2001) and > 20 vol. % (Ishii et al., 2019), respectively. Our model demonstrates that stishovite water solubility increases from 998 wt ppm at 14 GPa to 1317 wt ppm at 22 GPa along
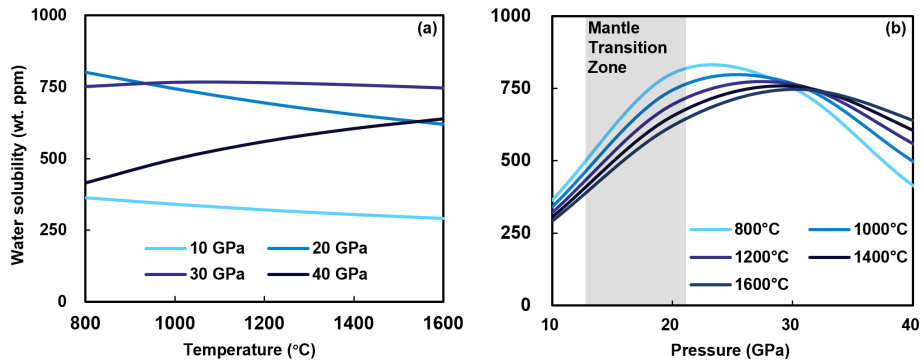
Figure 6. The impacts of **(a)** temperature and **(b)** pressure on water solubility in stishovite.
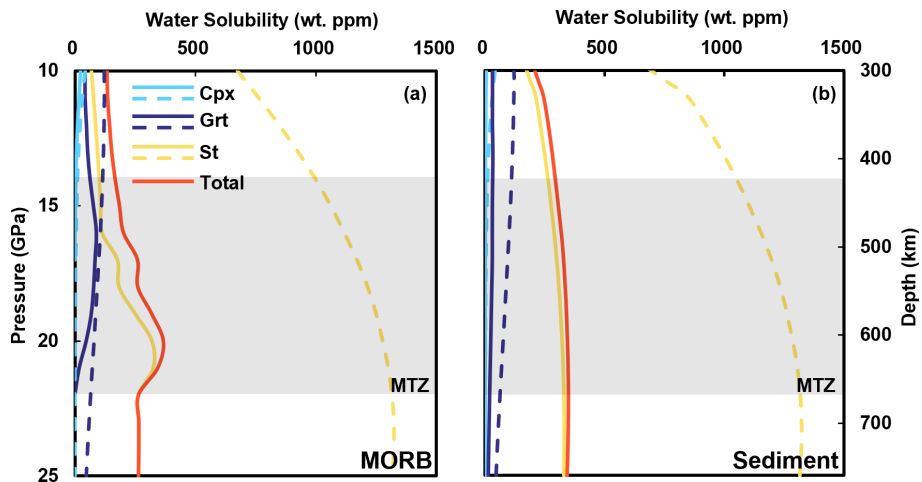

Figure 7. Water solubility in a cold subducted slab. Dashed lines represent water solubility of minerals, and solid lines show the actual water content considering mineral modal fractions (from Litasov and Ohtani, 2007) in subduction slabs. A cold subduction geotherm gradient from Litasov and Ohtani (2007) is used for the calculation (Table S2). The calculated result along with a hot subduction geotherm is presented in Fig. B1. The water solubility models used are Grt from Lu and Keppler (1997), Cpx from Gavrilenko (2008), and St from this study.

the cold subduction slab geotherm (Fig. 7). Consequently, stishovite may theoretically accommodate water released from the breakdown of hydrous minerals (Lin et al., 2020; Nisr et al., 2020; Walter, 2021). Due to a slight negative temperature dependence on water solubility of stishovite at 20 GPa (Fig. 6a), the water in stishovite will decrease with increasing temperature. That indicates a water outflow from stishovite along with the subducted slab being heated in the MTZ. In comparison to a hot subduction geotherm (Table S2 and Fig. B1), slabs will reduce more water in a cold subduction geotherm. Additionally, stishovite water solubility peaks at 22–32 GPa (corresponding conditions of the MTZ or topmost conditions of the lower mantle) (Fig. 6) and declines under higher-pressure conditions. Previous studies suggest that hydration of a large region of the transition zone and dehydration melting may act to trap H_2O in the transition zone (e.g., Schmandt et al., 2014). Taking into account the occurrence of melts, the optimal solubility likely falls within the water-rich mantle transition zone at pressures below 22 GPa.

Consequently, stishovite emerges as a key transporter supplying water to the mantle transition zone (Walter, 2021).

7 Conclusions and outlook

To sum up, the comprehensive review and exploration in this paper have encompassed water solubility in stishovite, hydrogen incorporation mechanisms, and governing factors. We have constructed a new model for water solubility in Al-bearing stishovite and delved into stishovite's role in transporting water through a subducting slab and implications for water distribution in the deep Earth. The key conclusions can be summarized as follows:

1. Water solubility in stishovite exhibits a positive correlation with Al content, which increases water concentrations via coupled substitution $Al^{3+} + H^+ \rightarrow Si^{4+}$ and enhances the incorporation of interstitial H_2O by Al

substitution-induced expansion of the stishovite structure.

2. The relationship between water solubility of Al-bearing stishovite and water fugacity, temperature, pressure, and Al content can be described as $C_{OH}^{St} = A \cdot f_{H_2O}^n \cdot \exp\left(-\frac{\Delta E + \Delta V \cdot P}{R \cdot T}\right) \cdot \exp\left(\frac{B \cdot X_{Al}}{R \cdot T}\right)$, with $n = 0.5$, $A = 24 \pm 13$ ppm GPa$^{-0.5}$, $\Delta E = -3.06 \pm 0.88$ kJ mol^{-1}, $\Delta V = 4.29 \pm 0.27$ cm^3 mol^{-1}, and $B = 7.69 \pm 1.12$ kJ mol^{-1}.

3. The calculation results from Eq. (2) demonstrate that stishovite's water solubility strongly depends on pressure, exhibiting a positive correlation below 22–32 GPa and a negative correlation above, indicating a peak solubility range at 22–32 GPa, while temperature dependence is weakly negative up to 30 GPa and weakly positive beyond.

4. Following a cold subduction slab geotherm, stishovite's water solubility increases from 998 wt ppm at 14 GPa to 1317 wt ppm at 22 GPa. This suggests that stishovite can potentially accommodate water released from the breakdown of hydrous mineral, contributing to the water-rich transition zone.

However, several crucial unanswered questions persist in research on water solubility of stishovite: (1) the solubility of Al and its impact on water solubility across varying pressure–temperature conditions requires clarification; (2) the roles of minor elements like Fe and Ti, as well as oxygen fugacity, remain unclear; (3) partitioning coefficients governing water distribution between stishovite and other major phases (e.g., Cpx, Grt, and melts) during slab subduction are not yet understood; and (4) Eq. (2) proposed in this paper needs refinement through systematic experiments conducted under controlled conditions. These issues are essential for understanding how water is transported into the deep Earth during subduction and require further detailed experimental and simulation-based investigations to address them.

Appendix A: Comparison between experimental and calculated results
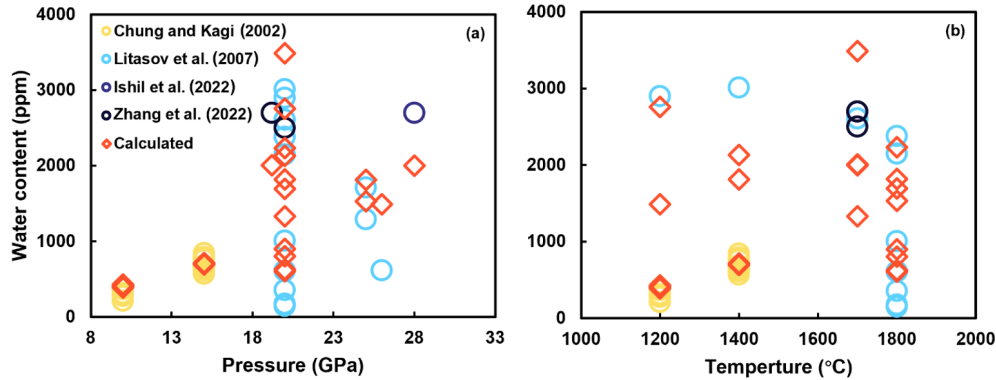
Figure A1. Comparison between experimental and calculated results (Table S1).

Appendix B: Water solubility of minerals in hot subducted slabs at 10–25 GPa
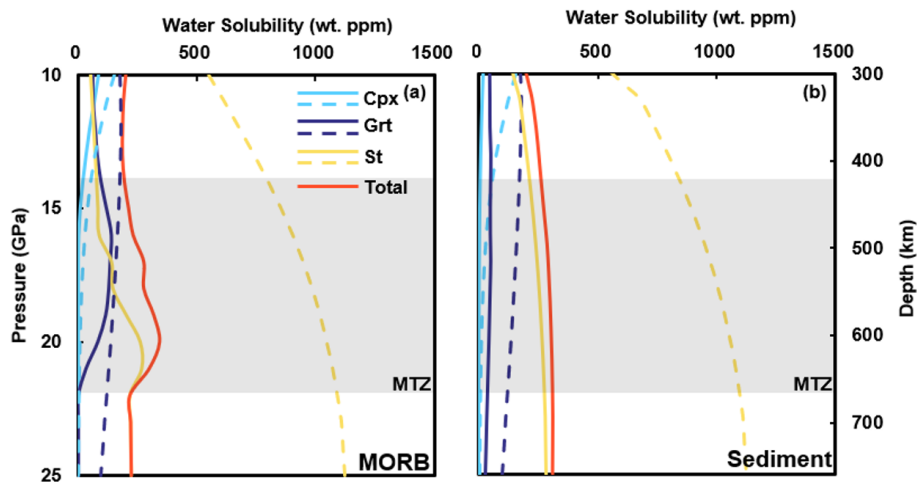
Figure B1. Water solubility in hot subducted slabs. Dashed lines represent water solubility of minerals, and solid lines show the actual water content considering mineral modal fractions (from Litasov and Ohtani, 2007). The water solubility models used are Grt from Lu and Keppler (1997), Cpx from Gavrilenko (2008), and St from this study.

References

Bell, D. R., Ihinger, P. D., and Rossman, G. R.: Quantitative analysis of trace OH in garnet and pyroxenes, Am. Mineralog., 80, 465–474, https://doi.org/10.2138/am-1995-5-607, 1995.

Bolfan-Casanova, N., Keppler, H., and Rubie, D. C.: Water partitioning between nominally anhydrous minerals in the MgO–SiO$_2$–H$_2$O system up to 24 GPa: implications for the distribution of water in the Earth's mantle, Earth Planet. Sc. Lett., 182, 209–221, https://doi.org/10.1016/S0012-821X(00)00244-2, 2000.

Bromiley, G. D., Bromiley, F. A., and Bromiley, D. W.: On the mechanisms for H and Al incorporation in stishovite, Phys. Chem. Mineral., 33, 613–621, https://doi.org/10.1007/s00269-006-0107-9, 2006.

Chao, E. C. T., Fahey, J. J., Littler, J., and Milton, D. J.: Stishovite, SiO$_2$, a very high pressure new mineral from Meteor Crater, Arizona, J. Geophys. Res., 67, 419–421, https://doi.org/10.1029/JZ067i001p00419, 1962.

Chung, J. I. and Kagi, H.: High concentration of water in stishovite in the MORB system, Geophys. Res. Lett., 29, 2020, https://doi.org/10.1029/2002GL015579, 2002.

Fischer, R. A., Campbell, A. J., Chidester, B. A., Reaman, D. M., Thompson, E. C., Pigott, J. S., Prakapenka, V. B., and Smith, J. S.: Equations of state and phase boundary for stishovite and CaCl$_2$-type SiO$_2$, Am. Mineralog., 103, 792–802, https://doi.org/10.2138/am-2018-6267, 2018.

Frigo, C., Stalder, R., and Ludwig, T.: OH defects in coesite and stishovite during ultrahigh-pressure metamorphism of continental crust, Phys. Chem. Mineral., 46, 77–89, https://doi.org/10.1007/s00269-018-0987-5, 2019.

Gavrilenko, P.: Water solubility in diopside, PhD thesis, 5 June 2008, Universität Bayreuth, Bayreuth, Germany, https://epub.uni-bayreuth.de/id/eprint/581 (last access: 8 February 2024), 2008.

Gu, T., Pamato, M. G., Novella, D., Alvaro, M., Fournelle, J., Brenker, F. E., Wang, W., and Nestola, F.: Hydrous peridotitic fragments of Earth's mantle 660 km discontinuity sampled by a diamond, Nat. Geosci., 15, 950–954, https://doi.org/10.1038/s41561-022-01024-y, 2022.

Gutzow, I., Pascova, R., Jordanov, N., Gutzov, S., Penkov, I., Markovska, I., Schmelzer, J. W. P., and Ludwig, F. P.: 3. Crystalline and Amorphous Modifications of Silica: Structure, Thermodynamic Properties, Solubility, and Synthesis, in: Glass, edited by: Schmelzer, J. W. P., De Gruyter, 137–196, https://doi.org/10.1515/9783110298581.137, 2014.

Holtstam, D., Broman, C., Söderhielm, J., and Zetterqvist, A.: First discovery of stishovite in an iron meteorite, Meteorit. Planet. Sci., 38, 1579–1583, https://doi.org/10.1111/j.1945-5100.2003.tb00002.x, 2003.

Irifune, T. and Ringwood, A. E.: Phase transformations in subducted oceanic crust and buoyancy relationships at depths of 600–800 km in the mantle, Earth Planet. Sc. Lett., 117, 101–110, https://doi.org/10.1016/0012-821X(93)90120-X, 1993.

Irifune, T., Sekine, T., Ringwood, A. E., and Hibberson, W. O.: The eclogite-garnetite transformation at high pressure and some geophysical implications, Earth Planet. Sc. Lett., 77, 245–256, https://doi.org/10.1016/0012-821X(86)90165-2, 1986.

Irifune, T., Ringwood, A. E., and Hibberson, W. O.: Subduction of continental crust and terrigenous and pelagic sediments: an experimental study, Earth Planet. Sc. Lett., 126, 351–368, https://doi.org/10.1016/0012-821X(94)90117-1, 1994.

Ishii, T., Kojitani, H., and Akaogi, M.: High-pressure phase transitions and subduction behavior of continental crust at pressure–temperature conditions up to the upper part of the lower mantle, Earth Planet. Sc. Lett., 357–358, 31–41, https://doi.org/10.1016/j.epsl.2012.09.019, 2012.

Ishii, T., Kojitani, H., and Akaogi, M.: Phase Relations of Harzburgite and MORB up to the Uppermost Lower Mantle Conditions: Precise Comparison With Pyrolite by Multisample Cell High-Pressure Experiments With Implication to Dynamics of Subducted Slabs, J. Geophys. Res.-Solid, 124, 3491–3507, https://doi.org/10.1029/2018JB016749, 2019.

Ishii, T., Criniti, G., Ohtani, E., Purevjav, N., Fei, H., Katsura, T., and Mao, H.: Superhydrous aluminous silica phases as major water hosts in high-temperature lower mantle, P Natl. Acad. Sci. USA, 119, e2211243119, https://doi.org/10.1073/pnas.2211243119, 2022.

Johnson, E. A.: Water in Nominally Anhydrous Crustal Minerals: Speciation, Concentration, and Geologic Significance, Rev. Mineral. Geochem., 62, 117–154, https://doi.org/10.2138/rmg.2006.62.6, 2006.

Kaminsky, F.: Mineralogy of the lower mantle: A review of 'super-deep' mineral inclusions in diamond, Earth-Sci. Rev., 110, 127–147, https://doi.org/10.1016/j.earscirev.2011.10.005, 2012.

Karato, S.: Rheology of the deep upper mantle and its implications for the preservation of the continental roots: A review, Tectonophysics, 481, 82–98, https://doi.org/10.1016/j.tecto.2009.04.011, 2010.

Keskar, N. R., Troullier, N., Martins, J. L., and Chelikowsky, J. R.: Structural properties of SiO$_2$ in the stishovite structure, Phys. Rev. B, 44, 4081–4088, https://doi.org/10.1103/PhysRevB.44.4081, 1991.

Kohlstedt, D. L., Keppler, H., and Rubie, D. C.: Solubility of water in the α, β and γ phases of $(Mg,Fe)_2SiO_4$, Contrib. Mineral. Petrol., 123, 345–357, https://doi.org/10.1007/s004100050161, 1996.

Kueter, N., Brugman, K., Miozzi, F., Cody, G. D., Yang, J., Strobel, T. A., and Walter, M. J.: Water speciation and hydrogen isotopes in hydrous stishovite: implications for the deep Earth water cycle, Contrib. Mineral. Petrol., 178, 48, https://doi.org/10.1007/s00410-023-02028-6, 2023.

Lakshtanov, D. L., Litasov, K. D., Sinogeikin, S. V., Hellwig, H., Li, J., Ohtani, E., and Bass, J. D.: Effect of Al^{3+} and H^+ on the elastic properties of stishovite, Am. Mineralog., 92, 1026–1030, https://doi.org/10.2138/am.2007.2294, 2007a.

Lakshtanov, D. L., Sinogeikin, S. V., Litasov, K. D., Prakapenka, V. B., Hellwig, H., Wang, J., Sanches-Valle, C., Perrillat, J. P., Chen, B., Somayazulu, M., Li, J., Ohtani, E., and Bass, J. D.: The post-stishovite phase transition in hydrous alumina-bearing SiO_2 in the lower mantle of the earth, P. Natl. Acad. Sci. USA, 104, 13588–13590, https://doi.org/10.1073/pnas.0706113104, 2007b.

Li, J., Lin, Y., Meier, T., Liu, Z., Yang, W., Mao, H., Zhu, S., and Hu, Q.: Silica-water superstructure and one-dimensional superionic conduit in Earth's mantle, Sci. Adv., 9, eadh3784, https://doi.org/10.1126/sciadv.adh3784, 2023.

Libowitzky, E.: The Structure of Hydrous Species in Nominally Anhydrous Minerals: Information from Polarized IR Spectroscopy, Rev. Mineral. Geochem., 62, 29–52, https://doi.org/10.2138/rmg.2006.62.2, 2006.

Libowitzky, E. and Rossman, G. R.: An IR absorption calibration for water in minerals, Am. Mineralog., 82, 1111–1115, https://doi.org/10.2138/am-1997-11-1208, 1997.

Lin, Y., Hu, Q., Meng, Y., Walter, M., and Mao, H. K.: Evidence for the stability of ultrahydrous stishovite in Earth's lower mantle, P. Natl. Acad. Sci. USA, 117, 184–189, https://doi.org/10.1073/pnas.1914295117, 2020.

Lin, Y., Hu, Q., Walter, M. J., Yang, J., Meng, Y., Feng, X., Zhuang, Y., Cohen, R. E., and Mao, H. K.: Hydrous SiO_2 in subducted oceanic crust and H_2O transport to the core-mantle boundary, Earth Planet. Sc. Lett., 594, 117708, https://doi.org/10.1016/j.epsl.2022.117708, 2022.

Litasov, K. D. and Ohtani, E.: Effect of water on the phase relations in Earth's mantle and deep water cycle, in: Advances in High-Pressure Mineralogy, Geological Society of America, https://doi.org/10.1130/2007.2421(08), 2007.

Litasov, K. D., Kagi, H., Shatskiy, A., Ohtani, E., Lakshtanov, D. L., Bass, J. D., and Ito, E.: High hydrogen solubility in Al-rich stishovite and water transport in the lower mantle, Earth Planet. Sc. Lett., 262, 620–634, https://doi.org/10.1016/j.epsl.2007.08.015, 2007.

Liu, L., Zhang, J., Green, H. W., Jin, Z., and Bozhilov, K. N.: Evidence of former stishovite in metamorphosed sediments, implying subduction to > 350 km, Earth Planet. Sci. Lett., 263, 180–191, https://doi.org/10.1016/j.epsl.2007.08.010, 2007.

Liu, L., Zhang, J. F., Cao, Y. T., Green, H. W., Yang, W. Q., Xu, H. J., Liao, X. Y., and Kang, L.: Evidence of former stishovite in UHP eclogite from the South Altyn Tagh, western China, Earth Planet. Sc. Lett., 484, 353–362, https://doi.org/10.1016/j.epsl.2017.12.023, 2018.

Liu, X., Nishiyama, N., Sanehira, T., Inoue, T., Higo, Y., and Sakamoto, S.: Decomposition of kyanite and solubil-ity of Al_2O_3 in stishovite at high pressure and high temperature conditions, Phys. Chem. Mineral., 33, 711–721, https://doi.org/10.1007/s00269-006-0122-x, 2006.

Liu, X. W., Xie, Z. J., Wang, L., Xu, W., and Jin, Z. M.: Water incorporation in garnets from ultrahigh pressure eclogites at Shuanghe, Dabieshan, Mineral. Mag., 80, 959–975, https://doi.org/10.1180/minmag.2016.080.034, 2016.

Lu, R. and Keppler, H.: Water solubility in pyrope to 100 kbar, Contrib. Mineral. Petrol., 129, 35–42, https://doi.org/10.1007/s004100050321, 1997.

Magni, V., Bouilhol, P., and Van Hunen, J.: Deep water recycling through time, Geochem. Geophy. Geosy., 15, 4203–4216, https://doi.org/10.1002/2014GC005525, 2014.

Ni, H., Zheng, Y. F., Mao, Z., Wang, Q., Chen, R.-X., and Zhang, L.: Distribution, cycling and impact of water in the Earth's interior, Natl. Sci. Rev., 4, 879–891, https://doi.org/10.1093/nsr/nwx130, 2017.

Nisr, C., Shim, S. H., Leinenweber, K., and Chizmeshya, A.: Raman spectroscopy of water-rich stishovite and dense high-pressure silica up to 55 GPa, Am. Mineralog., 102, 2180–2189, https://doi.org/10.2138/am-2017-5944, 2017.

Nisr, C., Chen, H., Leinenweber, K., Chizmeshya, A., Prakapenka, V. B., Prescher, C., Tkachev, S. N., Meng, Y., Liu, Z., and Shim, S. H.: Large H_2O solubility in dense silica and its implications for the interiors of water-rich planets, P. Natl. Acad. Sci. USA, 117, 9747–9754, https://doi.org/10.1073/pnas.1917448117, 2020.

Ono, S.: High temperature stability limit of phase egg, $AlSiO_3(OH)$, Contrib. Mineral. Petrol., 137, 83–89, https://doi.org/10.1007/s004100050583, 1999.

Ono, S., Ito, E., and Katsura, T.: Mineralogy of subducted basaltic crust (MORB) from 25 to 37 GPa, and chemical heterogeneity of the lower mantle, Earth Planet. Sc. Lett., 190, 57–63, https://doi.org/10.1016/S0012-821X(01)00375-2, 2001.

Ono, S., Suto, T., Hirose, K., Kuwayama, Y., Komabayashi, T., and Kikegawa, T.: Equation of state of Al-bearing stishovite to 40 GPa at 300 K, Am. Mineralog., 87, 1486–1489, https://doi.org/10.2138/am-2002-1026, 2002.

Ono, S., Kikegawa, T., Higo, Y., and Tange, Y.: Precise determination of the phase boundary between coesite and stishovite in SiO_2, Phys. Earth Planet. Inter., 264, 1–6, https://doi.org/10.1016/j.pepi.2017.01.003, 2017.

Panero, W. R. and Stixrude, L. P.: Hydrogen incorporation in stishovite at high pressure and symmetric hydrogen bonding in δ-AlOOH, Earth Planet. Sc. Lett., 221, 421–431, https://doi.org/10.1016/S0012-821X(04)00100-1, 2004.

Panero, W. R., Benedetti, L. R., and Jeanloz, R.: Transport of water into the lower mantle: Role of stishovite: Transport Of Water Into The Lower Mantle, J. Geophys. Res., 108, 2039, https://doi.org/10.1029/2002JB002053, 2003.

Paterson, M. S.: The determination of hydroxyl by infrared absorption in quartz, silicate glasses and similar materials, Bulletin de Minéralogie, 105, 20–29, https://doi.org/10.3406/bulmi.1982.7582, 1982.

Pawley, A. R., McMillan, P. F., and Holloway, J. R.: Hydrogen in Stishovite, with Implications for Mantle Water Content, Science, 261, 1024–1026, https://doi.org/10.1126/science.261.5124.1024, 1993.

Pearson, D. G., Brenker, F. E., Nestola, F., McNeill, J., Nasdala, L., Hutchison, M. T., Matveev, S., Mather, K., Silversmit, G., Schmitz, S., Vekemans, B., and Vincze, L.: Hydrous mantle transition zone indicated by ringwoodite included within diamond, Nature, 507, 221–224, https://doi.org/10.1038/nature13080, 2014.

Peslier, A. H., Schönbächler, M., Busemann, H., and Karato, S. I.: Correction to: Water in the Earth's Interior: Distribution and Origin, Space Sci. Rev., 212, 811–811, https://doi.org/10.1007/s11214-017-0420-2, 2017.

Petersen, S. E., Hoisch, T. D., and Porter, R. C.: Assessing the Role of Water in Alaskan Flat-Slab Subduction, Geochem. Geophy. Geosy., 22, e2021GC009734, https://doi.org/10.1029/2021GC009734, 2021.

Poli, S. and Schmidt, M. W.: Petrology of Subducted Slabs, Annu. Rev. Earth Planet. Sci., 30, 207–235, https://doi.org/10.1146/annurev.earth.30.091201.140550, 2002.

Rossman, G. R.: Studies of OH in nominally anhydrous minerals, Phys. Chem. Mineral., 23, 299–304, https://doi.org/10.1007/BF00207777, 1996.

Schmandt, B., Jacobsen, S. D., Becker, T. W., Liu, Z., and Dueker, K. G.: Dehydration melting at the top of the lower mantle, Science, 344, 1265–1268, https://doi.org/10.1126/science.1253358, 2014.

Shillington, D. J.: Water takes a deep dive into an oceanic tectonic plate, Nature, 563, 335–336, https://doi.org/10.1038/d41586-018-07335-8, 2018.

Smith, E. M., Shirey, S. B., Richardson, S. H., Nestola, F., Bullock, E. S., Wang, J., and Wang, W.: Blue boron-bearing diamonds from Earth's lower mantle, Nature, 560, 84–87, https://doi.org/10.1038/s41586-018-0334-5, 2018.

Smyth, J. R.: Hydrogen in High Pressure Silicate and Oxide Mineral Structures, Rev. Mineral. Geochem., 62, 85–115, https://doi.org/10.2138/rmg.2006.62.5, 2006.

Spektor, K., Nylen, J., Stoyanov, E., Navrotsky, A., Hervig, R. L., Leinenweber, K., Holland, G. P., and Häussermann, U.: Ultrahydrous stishovite from high-pressure hydrothermal treatment of SiO_2, P. Natl. Acad. Sci. USA, 108, 20918–20922, https://doi.org/10.1073/pnas.1117152108, 2011.

Spektor, K., Nylen, J., Mathew, R., Edén, M., Stoyanov, E., Navrotsky, A., Leinenweber, K., and Häussermann, U.: Formation of hydrous stishovite from coesite in high-pressure hydrothermal environments, Am. Mineralog., 101, 2514–2524, https://doi.org/10.2138/am-2016-5609, 2016.

Stishov, S. M. and Popova, S. V.: A new dense modification of silica, Geokhimiya, 10, 923–926, 1961.

Thomas, R., Davidson, P., Rericha, A., and Recknagel, U.: Discovery of Stishovite in the Prismatine-Bearing Granulite from Waldheim, Germany: A Possible Role of Supercritical Fluids of Ultrahigh-Pressure Origin, Geosciences, 12, 196, https://doi.org/10.3390/geosciences12050196, 2022.

Thomas, S. M., Koch-Müller, M., Reichart, P., Rhede, D., Thomas, R., Wirth, R., and Matsyuk, S.: IR calibrations for water determination in olivine, r-GeO2, and SiO2 polymorphs, Phys. Chem. Mineral., 36, 489–509, https://doi.org/10.1007/s00269-009-0295-1, 2009.

Walter, M. J.: Water transport to the core–mantle boundary, Natl. Sci. Rev., 8, nwab007, https://doi.org/10.1093/nsr/nwab007, 2021.

Wu, Y., Fei, Y., Jin, Z., and Liu, X.: The fate of subducted Upper Continental Crust: An experimental study, Earth Planet. Sc. Lett., 282, 275–284, https://doi.org/10.1016/j.epsl.2009.03.028, 2009.

Xia, Q. K., Chen, D. G., Deloule, E., and Zhi, X. C.: Hydrogen isotopic compositions of mantle-derived megacrysts from cenozoic basalts, Eastern China, Chin. Sci. Bull., 43, 146–146, https://doi.org/10.1007/BF02891632, 1998.

Yan, B., Liu, S., Chastain, M. L., Yang, S., and Chen, J.: A new FTIR method for estimating the firing temperature of ceramic bronze-casting moulds from early China, Sci. Rep., 11, 3316, https://doi.org/10.1038/s41598-021-82806-z, 2021.

Yang, J. S., Dobrzhinetskaya, L., Bai, W. J., Fang, Q. S., Robinson, P. T., Zhang, J., and Green, H. W.: Diamond- and coesite-bearing chromitites from the Luobusa ophiolite, Tibet, Geology, 35, 875, https://doi.org/10.1130/G23766A.1, 2007.

Yang, X.: Effect of oxygen fugacity on OH dissolution in olivine under peridotite-saturated conditions: An experimental study at 1.5–7 GPa and 1100–1300 °C, Geochim. Cosmochim. Ac., 173, 319–336, https://doi.org/10.1016/j.gca.2015.11.007, 2016.

Yang, X. and Li, Y.: High-P/T experimental studies and water in the silicate mantle, Sci. China Earth Sci., 59, 683–695, https://doi.org/10.1007/s11430-015-5241-0, 2016.

Yoshino, T., Shimojuku, A., and Li, D.: Electrical conductivity of stishovite as a function of water content, Phys. Earth Planet. Inter., 227, 48–54, https://doi.org/10.1016/j.pepi.2013.12.003, 2014.

Zhang, K., Liu, H., Ionov, D. A., and Yang, X.: Effects of Oxygen Fugacity on Hydroxyl Incorporation in Garnet at 1–3 GPa and 800–1000 °C and Implications for Water Storage in the Mantle, J. Geophys. Res.-Solid, 127, e2022JB023948, https://doi.org/10.1029/2022JB023948, 2022.

Zhang, Y., Fu, S., Karato, S., Okuchi, T., Chariton, S., Prakapenka, V. B., and Lin, J.: Elasticity of Hydrated Al-Bearing Stishovite and Post-Stishovite: Implications for Understanding Regional Seismic V_S Anomalies Along Subducting Slabs in the Lower Mantle, J. Geophys. Res.-Solid, 127, e2021JB023170, https://doi.org/10.1029/2021JB023170, 2022.

Zhao, Y. H., Ginsberg, S. B., and Kohlstedt, D. L.: Solubility of hydrogen in olivine: dependence on temperature and iron content, Contrib. Mineral. Petrol., 147, 155–161, https://doi.org/10.1007/s00410-003-0524-4, 2004.

Zheng, Y., Chen, R., Xu, Z., and Zhang, S.: The transport of water in subduction zones, Sci. China Earth Sci., 59, 651–682, https://doi.org/10.1007/s11430-015-5258-4, 2016.